Available online at www.sciencedirect.com
SCIENCE DIRECT®
Deep-Sea Research I 53 (2006) 528–546
DEEP-SEA RESEARCH PART I
www.elsevier.com/locate/dsr

Instruments and Methods

Monitoring the integrated deep meridional flow in the tropical North Atlantic: Long-term performance of a geostrophic array

Torsten Kanzow[a,b,*], Uwe Send[a,c], Walter Zenk[a], Alan D. Chave[d], Monika Rhein[e]

[a]*Leibniz-Institut für Meereswissenschaften, Düsternbrooker Weg 20, 24105 Kiel, Germany*
[b]*National Oceanography Centre, Empress Dock, Southampton, SO14 3ZH, UK*
[c]*Scripps Institution of Oceanography, University of California San Diego, La Jolla, CA 92093-0230, USA*
[d]*Woods Hole Oceanographic Institution, Woods Hole, MA 02543, USA*
[e]*Institut für Umweltphysik, Otto Hahn Allee NW1, 28334 Bremen, Germany*

Received 7 September 2004; received in revised form 1 November 2005; accepted 27 December 2005

Abstract

As a component of the meridional overturning variability experiment in the tropical North Atlantic, a four-year-long time series of meridional transport of North Atlantic deep water has been obtained from moored end point measurements of density and bottom pressure. This study presents a quality assessment of the measurement elements. Rigorous pre- and post- deployment in situ calibration of the density sensors and subsequent data processing establish an accuracy of O(1.5 Sv) in internal transport in the 1200–5000 dbar range at subinertial time scales. A similar accuracy is reached in the bottom pressure-derived external transport fluctuations. However, for pressure, variability with periods longer than a deployment's duration (presently about one year) is not measurable. This effect is demonstrated using numerical simulations and a possible solution for detecting long-term external transport changes is presented.

Keywords: Geostrophic transport; Time series; Bottom pressure; Density; Meridional overturning circulation

1. Introduction

To lowest order, mid-latitude, subinertial oceanic motions are geostrophic, which admits a simple relationship between pressure and the mass flux per unit vertical distance (Pedlosky, 1987)

$$p(\xi_1) - p(\xi_0) = f \int \vec{k} \cdot (\rho \vec{v} \times \mathrm{d}\vec{r}), \qquad (1)$$

where ξ_0 and ξ_1 are two points in the horizontal plane such that $p(\xi_1) > p(\xi_0)$, k is the unit upward vector, ρ is the density of seawater, $\mathrm{d}\vec{r}$ is parallel to an arbitrary curve running from ξ_0 to ξ_1, and f is the Coriolis parameter. From (1), pressure is an integral measure of the horizontal water velocity $\vec{v}_\mathrm{h}$. It is this spatial low pass filtering which enables mapping of oceanic flows using hydrographic (temperature and salinity versus depth) data. Further, bottom pressure measurements (but not pressure in the upper ocean) discriminate depth-independent (barotropic) from baroclinic motions even in regions with energetic baroclinic variability, accounting for the typically large horizontal coherence scale of the

*Corresponding author. Tel.: +44 23 80596430; fax: +44 23 80596240.
E-mail address: tok@noc.soton.ac.uk (T. Kanzow).

0967-0637/$ - see front matter © 2006 Elsevier Ltd. All rights reserved.
doi:10.1016/j.dsr.2005.12.007

bottom pressure field in the open ocean (Luther and Chave, 1993).

In applying the geostrophic relation (1), there is no requirement to resolve the complicated horizontal structure of the velocity field to recover the net flow across a plane defined by the endpoints ξ_0 and ξ_1. This remains true even in the absence of strong correlation between pressure measurements, and hence offers an advantage over classic direct (e.g., current meter) observations, especially in climate monitoring applications where transport through up to basin-scale sections is of interest (Kanzow, 2000; Send et al., 2002; Hirschi et al., 2003; Johns et al., 2005). The pressure difference in (1) only gives the horizontally integrated velocity at the level where the measurements are carried out. To obtain a vertically integrated transport, information about the vertical structure of the horizontal velocity is required.

Because absolute horizontal pressure gradients cannot be accurately measured, it is standard procedure to determine the horizontal internal (depth varying) geostrophic flow field relative to the external (depth-invariant) velocity at some depth level through profiles of density measurements during hydrographic surveys. Such measurements lack the external velocity at the reference level and have an inherently low temporal sampling rate, as data collection is ship time intensive and hence hydrographic sections are only repeated at infrequent and often irregular intervals. This limitation has led to the use of moored measurements of the time-varying temperature and salinity fields, from which the internal velocity can be derived. In combination with co-located bottom pressure measurements, this enables the fluctuating velocity field and transport across a section defined by pairs of mooring endpoints to be obtained.

An early application of this technique was presented by Whitworth (1983), who used pressure and hydrographic data from the Drake Passage to infer transports. In another study, time series of geostrophic transport were compared with simultaneous current meter measurements in a closely spaced array across the deep western boundary current in the subtropical North Atlantic (Johns et al., 2005). The results demonstrate that the different measurements are in good agreement on time scales longer than 10 days. The present study is based on the meridional overturning variability experiment (MOVE) in the tropical Northwest Atlantic Ocean which is an on-going multiyear moored geostrophic experiment based on this methodology. In contrast to the study of Johns et al. (2005), where time-varying vertical density profiles were determined from temperature data, but salinity was derived via an empirical T–S relationship, in situ temperature and salinity variations were simultaneously measured during MOVE, which enables inference of in situ density fluctuations with higher accuracy. In operation since February 2000, the MOVE array has been serviced at approximately annual intervals (see Table 1). After four years of operation, the aggregate time series and calibration data acquired during service cruises offer a unique basis for analysis of the long-term performance of the method and evaluation of its applicability to long-term monitoring studies. Time series of internal transports have also been inferred from bottom mounted inverted echo sounder (IES) observations (e.g. Meinen and Watts, 1998, 2000; Watts et al., 2001; Book et al., 2002).

Table 1
Schedule of cruise carried out within the framework of MOVE

Date	Cruise	Task
February 2000	R/V Knorr 161	MOVE/GAGE deployment
January 2001	F/S Sonne 153	Recover/redeploy MOVE
February 2002	L'Atalante	Recover/redeploy MOVE
June 2003	F/S Sonne 172	Recover/redeploy MOVE
February 2004	F/S Meteor 60-4	Recover/redeploy MOVE

While beyond the scope of this paper, MOVE can be regarded as a pilot project to observe fluctuations of zonally integrated meridional mass transport of North Atlantic deep water (NADW), which is generally considered to be the deep southward branch of the Atlantic meridional overturning circulation. Because deep currents typically lack a remote sensing (e.g., satellite altimetry) signature, their long-term study requires the development of a reliable, cost-effective in situ monitoring methodology.

2. Experiment location and instrumentation

The MOVE experiment located at 16°N in the western basin of the Atlantic Ocean is designed to monitor fluctuations of the deep meridional flow on a range of time scales by means of horizontally-integrating endpoint moorings to give the internal and external velocity field and mass transport. The MOVE location was selected to fulfill several

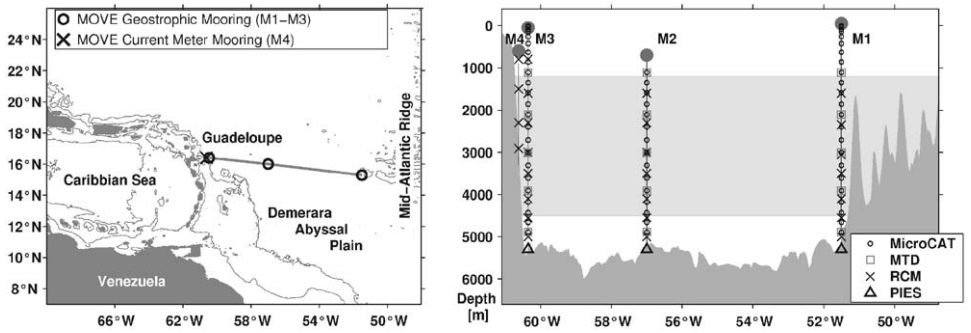

Fig. 1. Left panel: The MOVE array (M1–M4) located in the tropical Northwest Atlantic at 16°N is bounded by the Lesser Antilles Arc (Guadeloupe) to the west and the Mid-Atlantic Ridge (Researcher Rise) to the east. Right panel: MOVE consists of three geostrophic moorings (M1–M3) equipped with density sensors (MicroCAT and MTD) and current meters (RCM) in the vertical as well as combined bottom pressure recorders/inverted echo sounders (PIES). A current meter only mooring (M4) is located on the western continental rise. The main target of MOVE is transport fluctuations in the NADW layer (gray shading).

geometric requirements. To the west, a steep continental slope was desired such that only a small fraction of the southward DWBC could pass through the section inshore of the geostrophic array M3–M1 (Fig. 1). This minimizes the required number of current meter moorings on the continental slope. To make the geostrophic monitoring methodology feasible, topography between M1 and M3 needed to be as simple as possible, and at a minimum never rise above the levels of the end point depths (i.e., ~5000 m). Further, to reduce transport errors from the geostrophic approximation, the array had to be deployed away from the equator and have a limited meridional extent to avoid ambiguity from the latitude dependence of f. Finally, the zonal extent of the array was required to cover the entire western basin of the Atlantic to capture possible deep interior recirculations, as observed by Lee et al. (1996), Chave et al. (1997), and Lux et al. (2001). The quasi-zonal section at approximately 16°N (Fig. 1, left) meets these requirements in an optimal manner. To the west, the array is bounded by the Lesser Antilles arc and to the east by the Researcher Rise (a westward extension of the Mid-Atlantic ridge).

Additional dynamic conditions had to be met for MOVE. As inference of transport fluctuations on interannual time scales is the main goal of MOVE, seasonal and higher frequency variability was required to be small. Model simulations suggest an increase in seasonal transport variability toward the subtropics. Further, although there are few convincing observational data showing significant southward flow in the ocean's interior at higher latitudes, some numerical model simulations indicate that the deep southward flow in the North Atlantic only becomes confined near the western boundary somewhere in the subtropics (Stammer et al., 2000). North of that latitude, a non-negligible fraction of the southward flow is found in the eastern basin. Accordingly, a more northward location of the experiment would require additional measurements in the eastern basin, involving significant additional resources.

The MOVE array consists of three tall geostrophic moorings (M3, M2, M1; see Fig. 1, right) originally covering the depth range from about 1200–5000 m. Each mooring was instrumented with 15 MicroCAT temperature and conductivity recorders. The vertical sampling interval is 200 m at the top, then increasing to about 330 m at mid depth and then gradually decreasing to 200 m toward the bottom. Based on simulations using historical CTD data (Kanzow, 2000), this optimized arrangement has proven to yield smaller vertical sampling errors than would ensue from a uniform sensor spacing (Section 3 for details). From the third deployment period (February 2002) on, instrumentation at M3 and M1 was extended up to the sea surface using an additional 7 MicroCATs. In addition, up to 5 temperature and pressure loggers (MTP) were attached to each mooring (with a uniform vertical spacing) to give vertical mooring motion induced by ocean currents. Together with a mooring design program, MicroCAT conductivities (C) and temperatures (T) can thus be assigned depths with an accuracy of ± 3 m, and the corresponding salinities can be derived. These data allow the calculation of time-dependent profiles of dynamic height $\Delta\Phi(P,t) = \int_{P_{\mathrm{ref}}}^{P} \delta(P,t)\,\mathrm{d}P$ as defined by the pressure

integral of the specific volume anomaly δ. Finally the internal geostrophic velocity (horizontally integrated between pairs of sites) may be derived as follows:

$$v_{\mathrm{int}}(P,t) = \frac{1}{fL}\int_{P_{\mathrm{ref}}}^{P} [\delta(P,t)^A - \delta(P,t)^B]\,\mathrm{d}P, \qquad (2)$$

where t denotes time, f is the Coriolis parameter, L is the horizontal mooring separation, and P_{ref} represents a reference pressure.

At the base of each of the geostrophic moorings M1–M3, a bottom pressure sensor combined with an inverted echo sounder (PIES) was deployed. Beginning in 2001, additional Bourdon tube bottom pressure recorders were also deployed at M1 and M3. In this study, the PIES traveltime data will not be further considered. Theoretically, absolute geostrophic velocity can be calculated directly from pressure differences on an equigeopotential surface. Because neither those surfaces nor absolute pressure can be measured with sufficient accuracy, only relative (to the time-mean value, which is unknown) near-bottom (hereafter referred to as external) velocity fluctuations v'_{ext} can be obtained from the bottom pressure fluctuations P_{bot}. Simplifying (1) gives the standard relationship

$$v'_{\mathrm{ext}} = \frac{1}{\rho f L}[P'^{A}_{\mathrm{bot}} - P'^{B}_{\mathrm{bot}}]. \qquad (3)$$

The non-fluctuating part of the external velocity is ignored in this study.

Depth-dependent, horizontally-integrated geostrophic (internal plus external) velocity relative to a reference value may be obtained by adding the contributions from (2) and (3). In theory, a minimum requirement to determine the offset is a measurement of the horizontally-averaged velocity at one depth level at some point in time. If possible, the reference velocity measurement should be a vertical or a time average to minimize errors (Johns et al., 2005). Due to the difficulty in precisely relocating bottom pressure recorders between successive deployments, the offset will be different for each deployment period shown in Table 1.

The flow that passes the geostrophic array M3–M1 over the continental slope inshore of M3 has to be determined by direct current meter measurements at M3 and M4, which are located at the base and in the middle of the continental slope, respectively (Fig. 1). From the third deployment period onwards, an additional current meter mooring (M5) was deployed further to the west. The moorings M3, M2 and M1 were equipped with current meters at 6 depth levels (1600, 2300, 3000, 3600, 4100, 4600 and 4950 m). Mooring M4 (located at 3000 m water depth) covered 4 depth levels (800, 1450, 2250 and 2950 m) and M5 (located at 1600 m water depth) had two instruments (at 800 and 1450 m).

Data from five different types of moored sensors were acquired: MicroCAT, MTP, Aanderaa current meter, PIES and bottom pressure sensors based on Bourdon tubes. The MicroCATs, manufactured by Sea-Bird Electronics, carry an aged thermistor for temperature observations. Seawater conductivity is acquired by conductance measurements with an electrode cell. Some of the instruments are also equipped with pressure sensors from Druck Inc., which are based on piezoresistive silicon technology. The data return from the recovered MicroCATs has proven to be better than 95%.

The pressure sensor in the MTP is built by Keller AG and also makes use of piezoresistive technology. Its specified accuracy of 0.1% is comparable to that of the Druck sensors in the MicroCATs. The data return of the MTP has been better than 80%. The PIES, which are manufactured by Watts (URI), use a high precision Paroscientific pressure sensor based on dual beam quartz resonator technology. Paroscientific specifies the accuracy and resolution of its sensors as 0.01% and 0.0001% of full scale, respectively. The data return of the PIES is about 90%. Bourdon tube sensors with electro-optical feedback (Filloux, 1980) were also deployed. These devices have a sensitivity of 0.2 mm of water head and a very low noise level, but do not measure absolute pressure. They are equally reliable.

Initially, the majority of the Aanderaa current meters consisted of the well-known RCM8 type. These instruments still use the traditional rotor and vane that stalls at low current speeds and does not give the vector-averaged direction. Over time, these are being replaced with acoustic RCM9/11 instruments that do not have this limitation. The current meter data return is over 90%.

3. Calibration of temperature, conductivity and pressure

Prior to the first deployment in February 2000, the mooring design (i.e. the number of instruments and their locations) was simulated and optimized based on historical CTD data (Kanzow, 2000). The results showed that internal transport accuracy

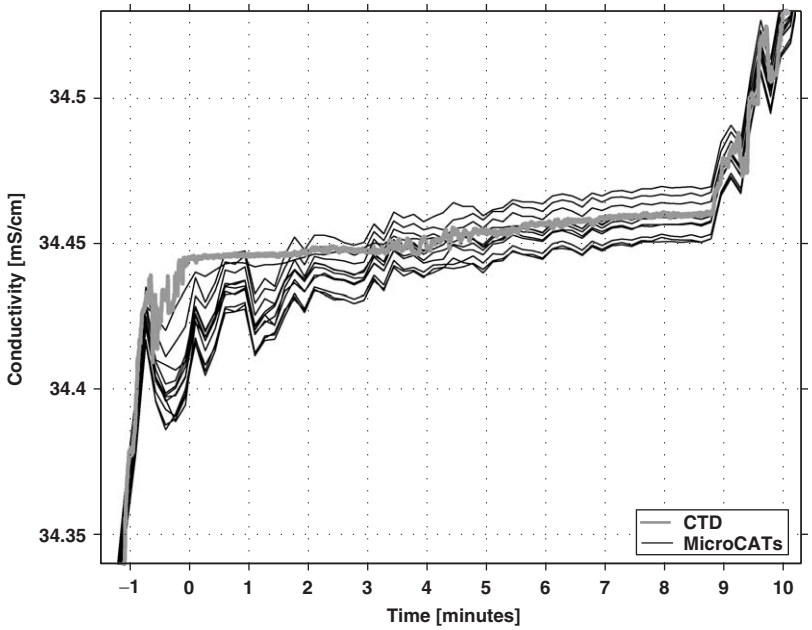

Fig. 2. Time series of conductivity during a bottle stop from the CTD probe (gray) and 12 MicroCATs (black).

from dynamic height of about 1.5 Sv ($1\,\mathrm{Sv} = 10^6\,\mathrm{m\,s^{-1}}$) in the depth range of 1200–5000 m can be achieved with about 15 MicroCATs if those deliver accuracies of 0.002 °C and 0.003 mS/cm $\equiv$ 0.003 psu, and if instantaneous depths are known to within $\pm$5 m. The error estimate incorporates uncertainties from sensor measurements as well as from vertical interpolation between the sampling points. This requires a continuous calibration program to meet the target baseline. The moored MicroCAT temperature (T) and conductivity (C) sensors, as well as the MTP pressure (P) sensors, were carefully calibrated in situ against a Seabird CTD probe before and after each deployment period (five times to date; see Table 1), and a linear drift correction was applied between these times. Laboratory calibration of the sensors is not feasible since all instrumentation is immediately redeployed on each cruise.

The reference CTD temperatures, conductivities and pressures were calibrated to the WOCE standard (Saunders et al., 1991) of $\pm$0.002 °C, $\pm$0.002 mS/cm and 0.02%, respectively. The goal of the MicroCAT calibration was to reduce the uncertainties in T and C to below 0.002 °C and 0.002 mS/cm relative to the CTD. This can only be achieved when the MicroCAT sensors exhibit a drift during a given deployment of no more than 0.01 °C or 0.01 mS/cm. Otherwise, the assumption of a predominantly linear drift during the deployment may not be a reasonable approximation.

In situ calibration was accomplished by attaching up to 14 MicroCATs at a time to the CTD rosette frame set to sample at their maximum rate (10 s) and then carrying out a cast. Best results were obtained when comparing MicroCATs against the CTD in the deep ocean below 2000 m. The surface mixed layer does not provide a stable enough environment to give the required accuracy, and the strong vertical temperature and conductivity gradients in the thermocline add strong depth-dependent offsets to the comparison.

Due to the equilibration time of the MicroCAT sensor (especially the conductivity cell) and the relatively low sample rate, accurate calibrations can only be obtained during bottle stops. Upon arriving at the depth of a particular bottle stop (minute 0), the CTD equilibrates almost immediately (Fig. 2). The large majority of the MicroCATs which were purchased prior to January 2000 (with the notable exception of one unit) display coherent fluctuations up to 4 min, which may be related to the internal electronics. Later versions of the instrument tend to adapt much more quickly, as can be seen from the smoother thin line in Fig. 2. While the CTD displays a conductivity change of $<$0.004 mS/cm during the first 4 min, the MicroCAT drift is typically $>$0.04 mS/cm. Accordingly, comparisons between

the CTD and MicroCATs were made more than 4 min after the start of a bottle stop (which should typically last about 8 min). For accurate calibration, conductivities from MicroCATs that do not have pressure sensors need to be depth corrected, as the conductivity cell geometry changes with applied pressure (SeaBird-Electronics, 2002). The equilibration time of several minutes is only relevant during the in situ calibration, and does not pertain during mooring operation where property variations display much smaller amplitudes and longer time scales.

This procedure yields a depth-independent offset between individual MicroCAT T and C measurements and the CTD probe. In Fig. 3, the individual offsets are shown for the five in situ calibrations that have been carried out to date. The MicroCAT temperature sensors have been very stable over 4 years and no temperature sensor has shown a mean deviation from the CTD reference of more than $\Delta T = 0.01\,^{\circ}C$. It is also obvious that almost all of the MicroCATs give a systematically higher temperature than the CTD instrument, with a mean offset between 0.002 and 0.004 °C (see top right panel of Fig. 3). There is no indication that the temperature calibration has changed significantly over 4 years, as the individual cruise standard deviation of ΔT remains constant in time. Thus, sensor stability over a given deployment of under 0.01 °C is readily achieved, yielding the desired temperature accuracy of 0.002 °C.

The deviation of conductivity of individual MicroCATs is generally less than $\Delta C = 0.01$ mS/cm. The few instruments that were proven to be unreliable were replaced. However, the conductivity measurements are extremely stable in time and a linear drift through each deployment period is a valid approximation. Accordingly, the individual conductivity cells display the temporal stability required to reach accuracies of 0.002 mS/cm after correction. The deployment mean ΔC increases slowly in time (from 0.002 to 0.004 mS/cm). The standard deviation of ΔC, which is a measure of stability, grows from 0.003 to 0.009 mS/cm over 4 years.

Overall, the MicroCATs exhibit outstanding long-term stability in temperature and conductivity, and better performance than specified by the manufacturer has been achieved. Individual small deviations can be removed such that the remaining error caused by linear drift correction is typically about 0.001 °C and 0.002 mS/cm relative to the CTD reference. The additional small offset from the CTD is not a problem because the calculation of geostrophic currents involves density differences, and the small offsets cancel out almost entirely.

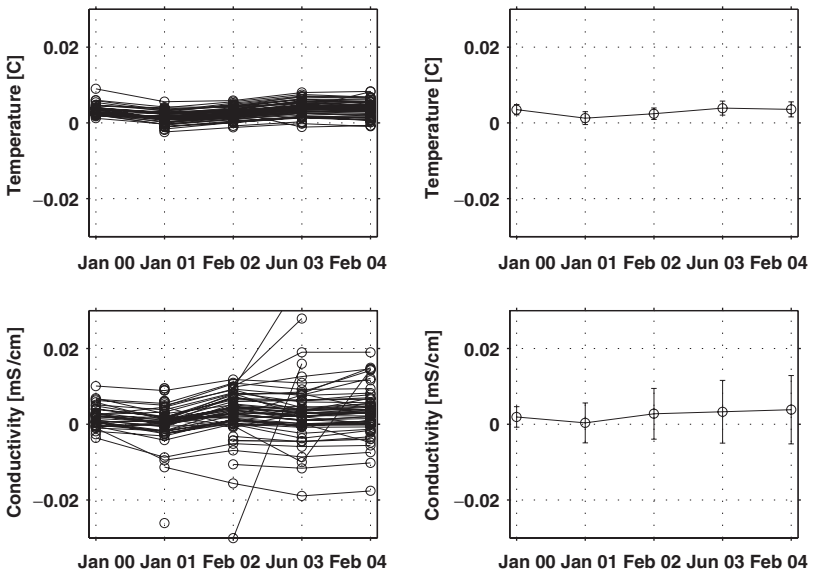

Fig. 3. In situ calibration: the MicroCAT minus CTD differences for temperature (top left panel) and conductivity (lower left panel) for all individual MicroCAT instruments as obtained during the five service cruises. Also shown is the cruise mean deviation for MicroCAT minus CTD and the standard deviation for temperature (top right panel) and conductivity (lower right panel).

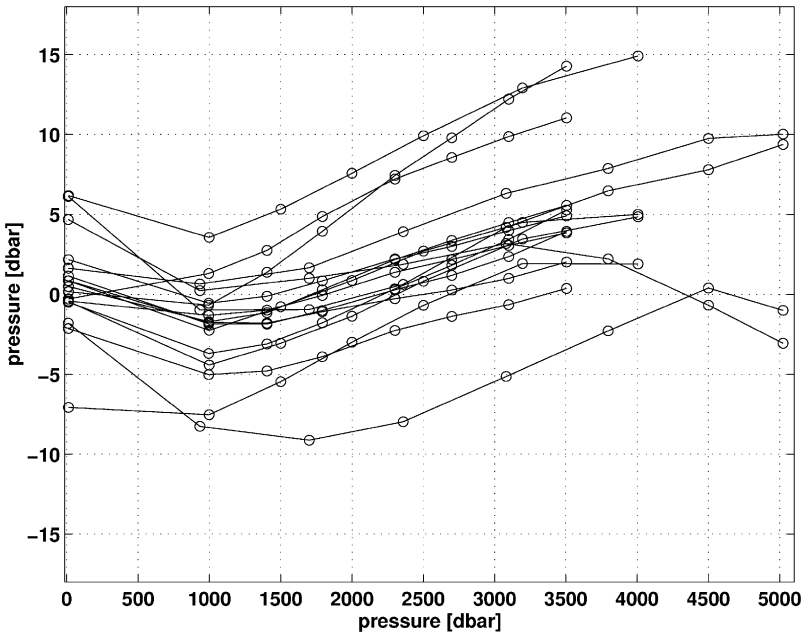

Fig. 4. In situ calibration: deviation of individual MTD pressures from the Sea-Bird CTD as obtained during calibration casts aboard F/S Meteor in February 2004.

The MTP pressures also have to be calibrated against the CTD to ensure exact, time-dependent depth assignment for the MicroCATs during each deployment. The pressure difference ΔP displays a depth dependence which has a similar shape for most instruments (Fig. 4). From the surface downward, ΔP first decreases and then increases below roughly 1000 m, so that at very large depths it turns back toward values lower than at the sea surface. It is important to correct every MTP sensor at the pressure where it will be operating. As pre-and post-deployment calibrations have been carried out, again a linear drift correction has been applied. The long-term stability of the MTP pressure calibration can be seen in Fig. 5. With the year-to-year differences in ΔP of individual instruments being generally <5 dbar, the linear drift correction should be able to provide MTP pressure time series with residual errors of about 1 dbar relative to the CTD standard. When calculating geostrophic velocities according to (3), CTD-induced pressure offsets cancel out.

4. Moored hydrographic data processing

To obtain internal velocity using (2), time series $S(P,t)$ and $T(P,t)$ at mooring sites M3, M2 and M1 have to be generated, from which $\delta(P,t)$ may be computed. To ensure high accuracy, careful depth assignment of the MTPs and MicroCATs is essential. When converting C to S, an inaccuracy in sensor depth of 20 m would result in an error in S of 0.01 psu. This precludes inference of sensor depth from water depth and mooring wire measurements.

Instead, the minimum (i.e., shallowest, corresponding to times of weakest flow velocity) values of each of the typically 5 MTP pressure time series at a given mooring are extracted. During such intervals, results from a static mooring simulation program (Berteaux, 1976) suggest that the mooring is oriented vertically. The pressures are converted to depths via the hydrostatic relation and compared with the nominal depths of the MTPs from the mooring construction plan, taking into account the vertical wire stretch due to tension (Helmbrecht, 2001). Note that the needed accuracy cannot be reached with nylon or other compliant mooring line material. Since errors in water depth typically dominate, a depth-independent offset between the nominal and the observed MTP depths is typical. By applying an offset correction, a match between the observed and the nominal depth with an accuracy of better than 3 dbar for an individual MTP can be achieved. Each MTP is co-located with a MicroCAT, hence at those points the T–C depth is known to better than 3 dbar. The depth of the other

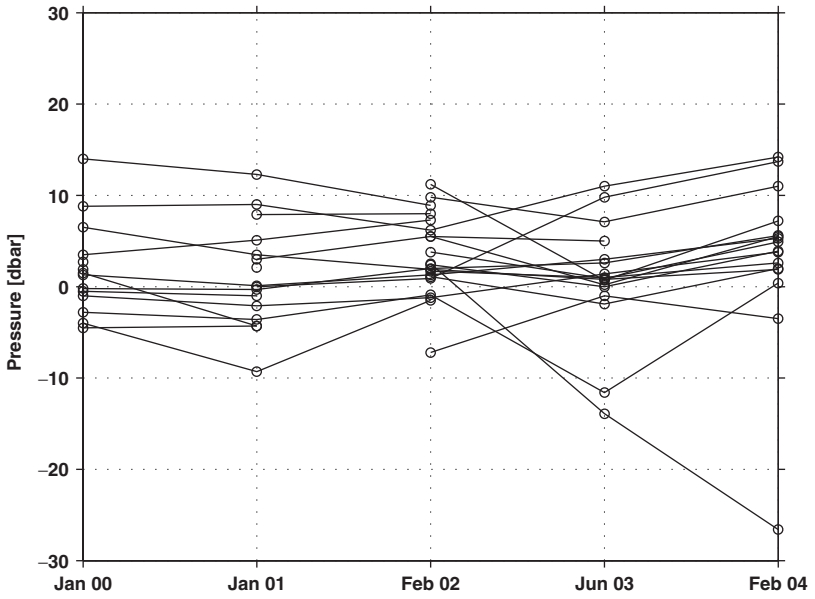

Fig. 5. Pressure deviation ΔP of individual MTDs from the Sea-Bird CTD obtained during the five service cruises. For the purpose of demonstration, ΔP has been evaluated at 3500 dbar to avoid ambiguity caused by its depth dependence.

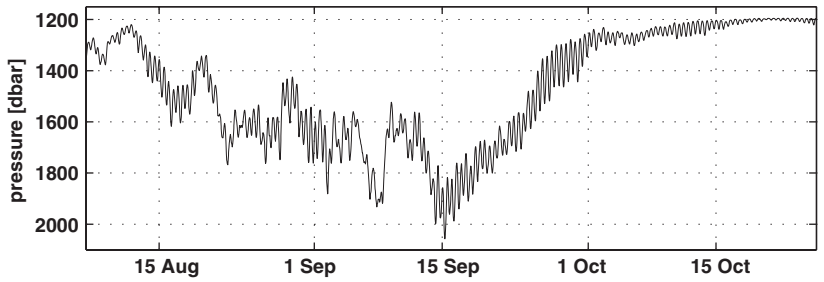

Fig. 6. Pressure time series of an MTP sensor (at a nominal depth of 1189 m) during an extremely strong current event in year 2000 at mooring M3.

MicroCATs can be inferred from the mooring design. The value of 3 dbar coming from the mismatch between the nominal and observed pressures is a realistic estimate for the residual depth assignment error.

After the static depth assignment, a correction for vertical mooring motion caused by ocean currents is carried out on a 2-hourly basis to resolve tidal periods. This can be very important when tidal flows amplify an already strong current event (see Fig. 6). In practice the MTP pressures are linearly interpolated onto the MicroCATs, so that for each instrument a pressure time series is obtained. Helmbrecht (2001) has shown that during strong current events, as displayed in Fig. 6, when the western boundary mooring M3 gets subducted by several hundred meters, simple linear vertical interpolation between the pressure sensors might yield errors of several tens of meters in the MicroCAT depths. During these events we combine the measured MTP pressures with the modeled mooring curvature (from the mooring simulation program forced by the measured velocities) for vertical interpolation of the MicroCAT positions between the MTP sampling points, which helps to reduce the uncertainty drastically. As an extreme test, Helmbrecht (2001) used only the shallowest and deepest MTP (located at 1200 and 4900 m, respectively) on mooring M3 during a very strong current event when it blew over by 750 m. The resulting deviations between predicted and measured depths of a third MTP (nominally at 3500 m)

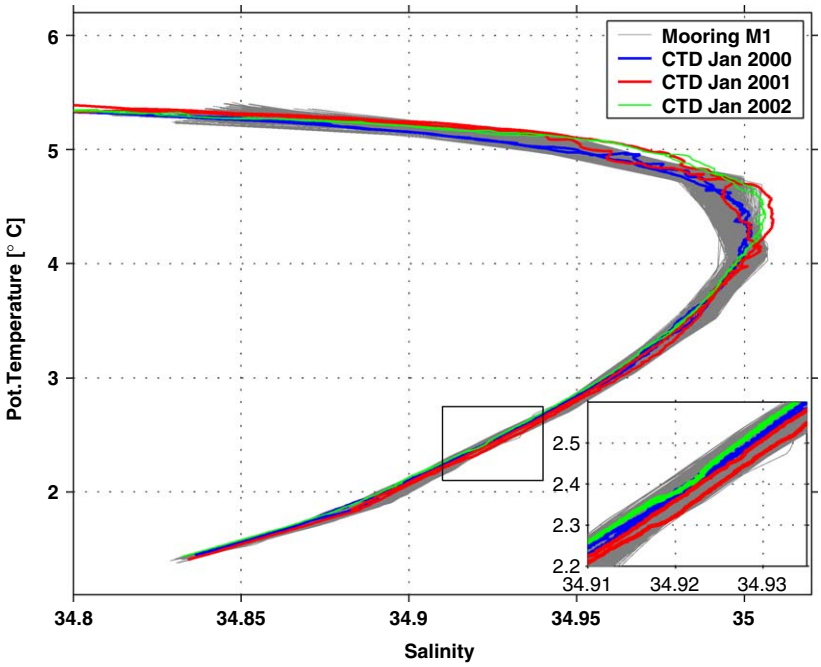

Fig. 7. θ–S diagram from the NADW/AABW depth range: daily profiles from mooring M1 from the year 2001 deployment period (gray). Superimposed are shipboard profiles acquired near M1 in January 2000, January 2001 and January 2002. The close agreement between lowered and moored measurements is confirmed by the inset in the lower right corner.

did not exceed 11 m at any time. Since in practice at least four MTP are available per mooring, even in extreme events MicroCAT depths can be inferred with a few meters of accuracy.

Finally, S can be computed from T, C, and P using standard methods. The final T and S time series are then 48-hour low-pass filtered (using a five pole Butterworth filter) and linearly interpolated onto a regular pressure and time grid with a resolution of 20 dbar and 12 h, respectively. The local T–S relationship within the NADW is generally stable enough for consistency checks in time (Johns et al., 2005). Comparing the moored T and S series to shipboard CTD data acquired in the vicinity of the moorings is a reliable way to perform a final quality check on the calibration and processing techniques. The example in Fig. 7 shows good agreement between the mooring and CTD data. A closer look reveals that in the temperature range above 3.5 °C, where the θ–S diagram displays strong curvature, the mooring curves cut across the CTD curves, which is a result of linear interpolation between the mooring sampling points. In simulations where the coarse MOVE vertical sampling configuration had been applied to high resolution CTD profiles, an r.m.s. error from the vertical linear interpolation of 0.0058 $m^2 s^{-2}$ in geopotential anomaly for the NADW range was found, which is about 50% larger than would be obtained using cubic splines for vertical interpolation of (Kanzow, 2000). However, when computing internal transports from mooring pairs, the resulting errors do not display significant interpolation technique-dependent differences since the biases caused by linear interpolation at both sites cancel out almost completely (Kanzow, 2000; Johns et al., 2005).

The final processed four-year time series of anomalies of T in Fig. 8 indicate that the patterns of variability clearly differ from site-to-site, with fluctuations being strongest at the western boundary (M3) and weakest at the easternmost site (M1). As will be discussed later, internal transport integrated across the whole section (M3–M1) is thus less contaminated by baroclinic Rossby waves and eddies than transport integrated across the west section (M3–M2). To demonstrate the consistency of the calibrations from one deployment to another, time series of geopotential anomaly (or dynamic height) from mooring M1 are displayed in Fig. 9. The course of the curve across the data gaps during service intervals (marked by dashed lines) displays no significant jumps.

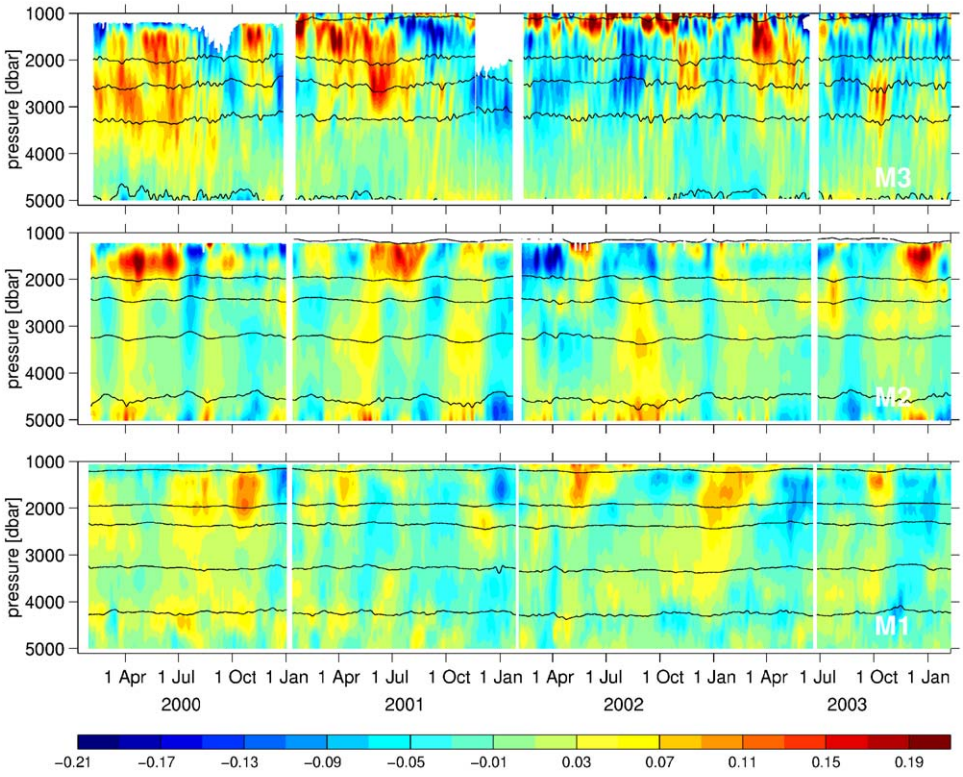

Fig. 8. Temperature anomalies from moorings M1 (east), M2 (center) and M3 (west) from January 2000 until February 2004. Gaps in January 2001, February 2002 and June 2003 are due to mooring service. Missing data in the upper NADW range from November 2001 to February 2002 are caused by mooring breakage. Superimposed are the density levels $\sigma_{1.5} = 34.42$, 34.70, 34.755 and $\sigma_4 = 45.83$ and 45.90.

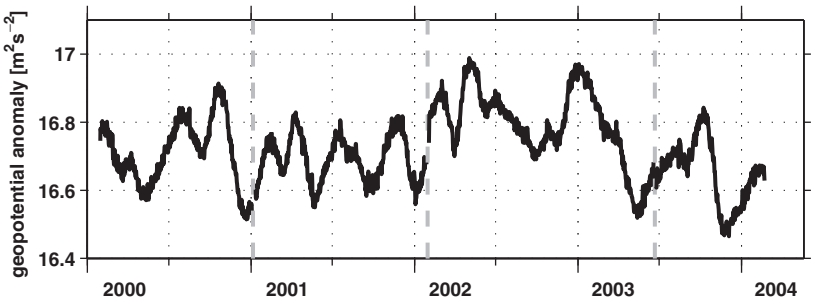

Fig. 9. Geopotential anomaly at 1200 dbar (relative to 4950 dbar) from mooring M1 between February 2000 and February 2004. The short data gaps resulting from mooring recovery and redeployment are marked by the gray dashed lines.

5. Bottom pressure

Both types of bottom pressure data were despiked and subsequently 48 h low-pass filtered (see Fig. 10, top) to suppress diurnal and semidiurnal tides. Each segment of the pressure time series exhibit monotonic long-term drift whose rate is generally largest at the beginning of the record. The Paroscientific sensors used in the PIES were detrended using the empirical exponential-linear relationship of Watts and Kontoyiannis (1990) $P^{\mathrm{PIES}}_{\mathrm{drift}}(t) = A(1 - \mathrm{e}^{Bt}) + Ct + D$ where t is time since recording began and A, B, C and D are free parameters estimated by least squares. For the Bourdon tube sensors, the long-term drift is explained by Mott creep (Filloux, 1980) which follows a power law $P^{\mathrm{Bourd}}_{\mathrm{drift}}(t) = \hat{A} + \hat{B}(t + \hat{C})^{D}$, where $\hat{A}$, $\hat{B}$, $\hat{C}$ and $\hat{D}$ represent the free parameters. The typical annual pressure drift rates

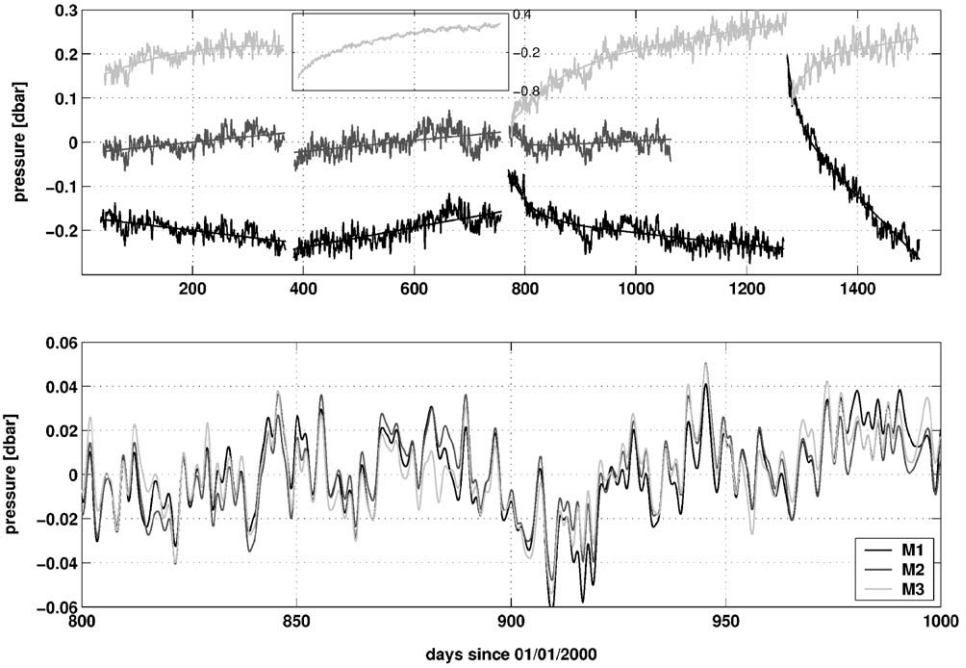

Fig. 10. Top: Bottom pressure fluctuations (mean subtracted and 48 h low-pass filtered) from sites M1, M2 and M3. Apart from the second time series at M3 , which comes from a Bourdon tube sensor (note the condensed scale), all of the other records were obtained from the PIES. For each time series, a least squares fit is displayed (see text for details). To enable easily distinction, arbitrary offsets have been added. Bottom: The same time series with trends subtracted in the time interval from day 800–1000. Note the extremely high correlation between M1, M2 and M3.

of the PIES are O(0.1) dbar (with the clear exception of the last time series at site M1) The Bourdon tube sensor drift (second time series at site M3) is about one order of magnitude larger (note the condensed scale in Fig. 10, top). After estimating and subtracting the drift, pressure time series at M3, M2 and M1 become almost indistinguishable from each other (Fig. 10, bottom). With a distance of 1000 km between M3 and M1, this implies large horizontal correlation scales of bottom pressure in the tropical North Atlantic, as has previously been described (e.g., Brown et al., 1975; Hughes and Smithson, 1996). The large coherence indicates that bottom pressure fluctuations at a sub-centimeter of water head scale can be accurately measured. Watts and Kontoyiannis (1990) claim that the stability over a few days and the resolution are better than 0.1 cm water head, which translates into a cross array transport discrepancy of less than 1 Sv.

However, neither empirical nor physics-based de-drifting can distinguish between sensor drift and a true long-period ocean signal. Due to the large amplitude of the drift at the beginning of the deployment, the fit applied is susceptible to short period ocean signals at the beginning of the time series. Further, it is be susceptible to ocean signals with periods on the order of the length of the time series itself.

A persistent problem is that larger uncertainty in the drift estimates at the beginning and end of each deployment segment makes it impossible to reliably concatenate them. The end-point matching technique of Whitworth and Peterson (1985), in which data segments from successive deployments are joined by matching low frequency components of the time series, will be especially susceptible to such error. Instead, successive data segments are simply strung together after their individual drifts are removed to obtain a quasi-continuous multi-annual pressure time series, as was also done by Meredith et al. (1996). However, this technique is bound to reduce any real interannual variability. Simulations in Appendix suggest that the use of a modified bottom pressure sensor deployment scheme may overcome this problem.

In Appendix, the effect of de-trending on long-term bottom pressure variability is simulated in more detail. The most important results are that the

annual cycle can only be partly recovered from annual data segments, and that multi-year uninterrupted time series lead to strong improvement. When overlapping segments are available, some skill exists for the assessment of variability on periods longer than the duration of individual segments. Additionally, on annual and longer time scales, bottom pressure measurements may be constrained by satellite altimetry (Schmidt, 2004). Assuming a typical error for a single sea surface height measurement of 2 cm, the annual mean anomaly (relative to a geoid model) may be determined within ± 2 mm with a weekly sample rate. To estimate bottom pressure changes from altimetry, the steric contribution to sea level change has to be subtracted. This in turn requires precise continuous sampling of the full water column vertical density structure which is subject to further uncertainty. Such measurements have been carried out in MOVE at M3 and M1. With the distances of the mooring sites to the nearest Jason tracks being significantly smaller than the baroclinic Rossby radius of about 60 km (the distances of M3 and M1 to a track are 10 and 30 km, respectively), one may be able to constrain interannual bottom pressure fluctuations to a certain degree using altimeter measurements.

Finally, before transport fluctuations are calculated from the bottom pressures using (3), the fortnightly (M_f) and monthly (M_m) tides are removed using a tidal harmonic fit from the T Tide toolbox (Pawlowicz et al., 2002), which yields amplitudes of about 0.0174 and 0.0080 dbar, respectively, in this region.

6. Transport

In the following, the different contributions to transport will be analyzed and assessed. The continuity of a time series between deployments is an important indicator of consistency and accuracy. Fig. 11 (top) shows the internal meridional

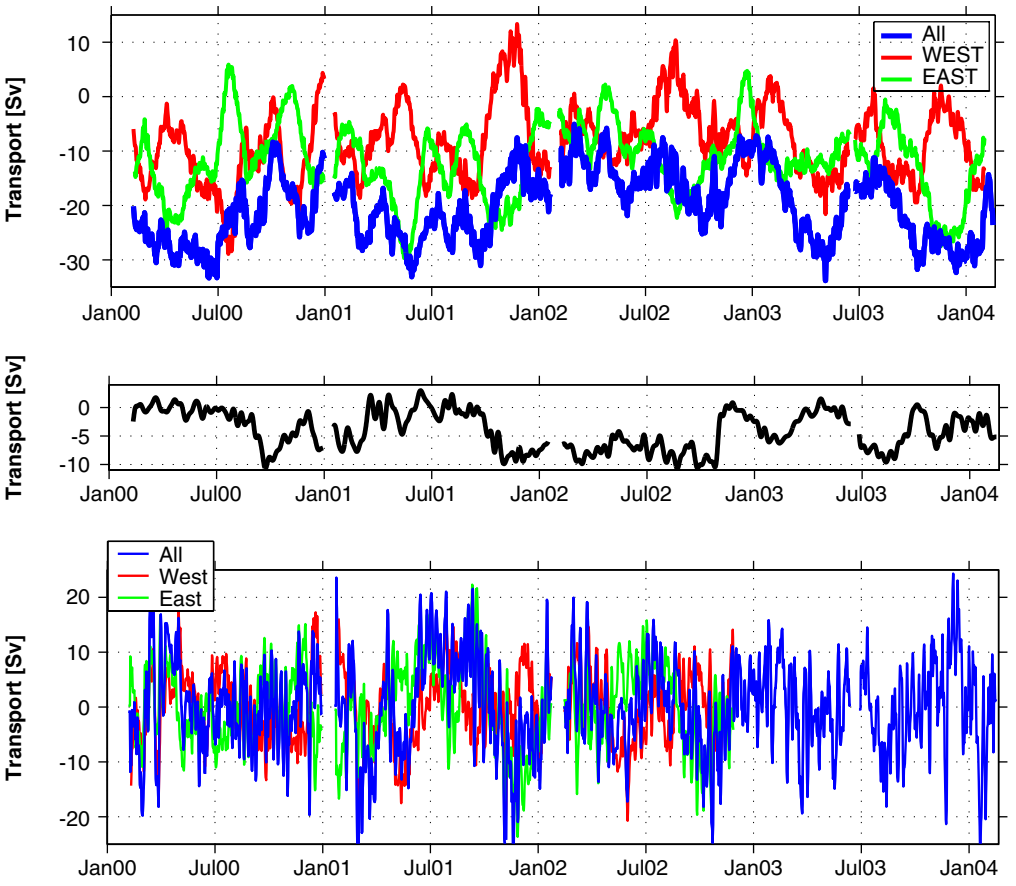

Fig. 11. Top: Internal transport below 1200 dbar relative to 5000 dbar. Center: Transport below 1200 dbar over the continental slope west of M3 from current meter measurements. Bottom: External (bottom pressure derived) transport fluctuations below 1200 dbar.

transport below 1200 dbar relative to 5000 dbar. At the break points, the transition from one deployment period to the next look consistent in all cases. This can best be verified at the eastern (M2–M1) end where the data gaps are shorter by several days compared to the western or whole section (M3–M2 or M3–M1) transport. These smooth transitions in an otherwise highly variable time series give confidence that the accuracy goal for internal transport of less than 1.5 Sv on subinertial time scales has been reached (Kanzow, 2000).

It should be noted that during times when the uppermost density sensor was below 1200 dbar at M3 (either due to loss of the top part of the mooring in November 2001 or during strong current events as seen in Fig. 8), the internal transport spanning the NADW cannot be calculated directly. During those intervals, the velocity shear was extrapolated upward from the topmost working density sensor to the 1200 dbar level. It is reassuring that even an upward extrapolation of more than 800 dbar during the last two months of the second deployment does not create an abrupt transition (see Fig. 11). Simulations based on the internal velocity time series imply that an upward extrapolation of about 500 dbar introduces an estimated r.m.s. error of about 0.8 Sv.

The internal transport highlights a major benefit of the overall MOVE monitoring strategy. The transport in the western and eastern part of the array displays a clear 180° out-of-phase behavior on time scales of a few months, with a typical peak-to-peak magnitude of order 10–20 Sv. Spectral analysis yields a squared coherence of larger than 0.6 with a phase shift of 180° in the 70–250 day band (where the zero coherence level at 95% significance is 0.3). Thus, a significant part of the variability within the basin cancels out in this band when the transport is integrated over the whole section (blue line).

This is confirmed in Table 2: the standard deviation of total internal transport is 6.0 Sv and thus is somewhat lower than the western and eastern contributions of 6.3 and 6.4 Sv, respectively. Further, while the western and eastern contributions are dominated by baroclinic Rossby wave-induced fluctuations of about 90 days period (Kanzow, 2004), the total internal transport displays variability on longer time scales (Fig. 11, top). This confirms an ability to eliminate contributions from eddies, waves, and recirculations over the western basin of the North Atlantic, resulting in an increased signal-to-noise ratio of the low frequency, large-scale variability. From simulations carried out with output from the FLAME ocean general circulation model with 1/3° horizontal resolution (Eden and Willebrand, 2001), it was found that interannual transport fluctuations below 1200 m integrated across the western basin only versus integration across the whole Atlantic along 16°N display a correlation of 0.73 (Kanzow, 2004). Thus, on these time scales, MOC fluctuations should be detectable by MOVE. Furthermore, simulations suggest that the signal-to-noise ratio of the internal transport could be increased significantly on all time scales if the MOVE transect was extended into the eastern basin (Kanzow, 2004).

Table 2
Mean, standard deviation and accuracy of observed transports in Sv below 1200 dbar

Transport	Mean	Std. Dev.	Accuracy
Internal (M1–M3)	−20.1	6.0	1.5
Internal (M2–M3)	−11.6	6.3	1.5
Internal (M1–M2)	−8.5	6.4	1.5
External (M1–M3)	0.0	8.4	2.0
External (M2–M3)	0.0	7.0	2.0
External (M1–M2)	0.0	7.6	2.0
Boundary (W of M3)	−4.0	3.4	0.3
Internal (M1–M3 + boundary)	−24.1	4.6	1.6

Internal transport is given relative to 5000 dbar.

The DWBC is thought to be responsible for major parts of southward NADW flow (e.g. Hogg, 2001). The MOVE measurements indicate that the DWBC at 16°N is a jet of less than 100 km width located near M3, with southward velocity exceeding 50 cm/s at times. Thus, the transport through the boundary triangle over the continental slope west of M3 is important. It was obtained by interpolation of directly measured currents at M4, M3 (and when available, M5) and extrapolation of the horizontal shear toward the western boundary (see Fig. 11, middle panel). For this purpose, precise topography on the continental slope as acquired from the multibeam Hydrosweep echo sounder system aboard F/S SONNE was used. The observations imply that the flow is largely dominated by the DWBC. Periods of strong flow are observed from October 2000 to March 2001 and from October 2001 to November 2002. The February 2000 to June 2003 time mean southward transport below 1200 m over the slope amounts to 4.0 Sv with a standard deviation of 3.4 Sv. During times of weak flow inshore, an increased southward internal transport can be

observed further offshore (compare Fig. 11, top). As a result the standard deviation of total internal plus boundary triangle transport amounts to only 4.6 Sv, and thus is significantly lower than the variability of the internal transport alone (Table 2). We interpret this to be the signature of the DWBC meandering in the offshore direction, which has previously been observed at 26.5°N (e.g. Lee et al., 1996; Chave et al., 1997).

In order to estimate the uncertainty of the boundary triangle transport, different extrapolation schemes were tested, including no flow at the boundary and no velocity shear between the westernmost mooring and the boundary, yielding nearly identical results. Further, the transport measurement improvement from including M5 (which was only available during the third and fourth deployments) is almost negligible. From these tests, an uncertainty of 0.3 Sv in the boundary triangle transport has been derived.

The external near-bottom velocity fluctuations are obtained from bottom pressure according to (3). They are scaled to transport by multiplication by the mooring separation and NADW thickness of 3723 m between 1200 and 5000 dbar. Based on an error estimate in bottom pressure of about 2 mm of water head (obtained by comparing simultaneous pressure records at one site and as confirmed by Watts and Kontoyiannis, 1990), the resulting uncertainty for the external transport is 2 Sv. By construction the transport across each section has a zero mean, and the standard deviations amount to 8.0, 7.6 and 7.0 Sv for the whole, east and west sections, respectively. These numbers show that east and west transports are not independent. After November 2002, only transport for the whole section could be inferred due to problems with the PIES at M2. The time series are dominated by fluctuations on short time scales (<20 days) and at periods of a few months (Fig. 12 bottom). A closer look reveals that the high frequency fluctuations of the western and eastern contribution are highly coherent and thus might reflect large horizontal scale barotropic Rossby waves. On monthly time scales, the east and west transports are out of phase. This is a typical signature of eddies or waves with a scale shorter than the mooring separation, but could also reflect the spin-up and spin-down of an interior recirculation (Lee et al., 1996; Lux et al., 2001). Judging the consistency of the transition from one data segment to the next is more difficult for the external transport due to the presence of high-frequency fluctuations. However, a closer looks reveals the general continuity of the longer period signals across the data gaps. Thus, the drift removal of the bottom pressure time series appears to have worked satisfactorily, although the simulations in Appendix show that a hypothetical interannual variability might be suppressed.

External transport does not appear to be correlated with the internal transport at any period. This has also been observed in the North Atlantic Current by Meinen (2001). Kanzow (2004) interprets the internal and external contributions at 16°N to be dominated by the baroclinic and barotropic components of the dynamics, respectively.

7. Concluding remarks

The first four years of the MOVE mass transport time series have been presented with a focus on measurement accuracy and the long-term performance of the experiment. The fact that MOVE comprises several consecutive deployment periods allows for a detailed analysis of the consistency of the data set.

Analysis of the temperature, conductivity and pressure calibration suggests that instantaneous internal transport accuracy of better than 1.5 Sv in the 1200–5000 dbar layer can be achieved. The basis for this statement is the long-term stability of the conductivity, temperature and pressure sensors. In particular, the low drift rate of the conductivity measurements is significantly better than was expected. If the in situ calibration referenced against a CTD standard is carried out with care, drift removal (relative to the CTD) of 0.002 mS/cm, 0.001 °C and 1 dbar over an annual deployment period can be attained. Further, instrument depth assignment and mooring motion correction, which are key elements for accurate time-dependent density measurements, have been applied to within a few meters accuracy down to 5000 m depth.

To reach comparable transport accuracy with a classical current meter array, the baroclinic Rossby radius of about 60 km would need to be resolved, which would require about 20 moorings. Finally, it was demonstrated that basin-scale integration across the western North Atlantic increases the signal-to-noise ratio of the long period fluctuations.

The transports through the narrow boundary triangle west of M3, which are not captured by the geostrophic array (M3–M1), have been acquired by current meter measurements. In this environment of

strong currents, the consistency of the successive data segments shows that these measurements have been obtained with sufficient accuracy. Further, a clear relationship between temporal changes in boundary and internal transports has been demonstrated. This is a further indication of the consistency of both measurement components.

The highly variable external fluctuations have to be treated with special care. On the one hand, 1200–5000 dbar transport fluctuations with time scales up to about 6 months can be obtained by bottom pressure measurements with an accuracy of 2 Sv. A resolution of better than 1 Sv can be reached (corresponding to a velocity of 0.3 mm/s) when a mooring separation of 1000 km is used. On the other hand, the simulations in Appendix indicate that with the present technique of detrending and concatenating annual data segments, longer period variability must necessarily be underestimated. It is not clear to what extent true interannual variability is present in the bottom pressure gradient (or external transport) at the MOVE section. Simulations suggest that longer deployment durations and temporally overlapping data segments can significantly increase the skill for estimating the long-term evolution of the external transport fluctuations. This strategy will be pursued during future deployments. The PIES can remain on the seafloor for several years. As the newest versions are equipped with an acoustic telemetry system, bottom pressure data can be transmitted to a vessel passing by without having to recover the instruments each time. At the same time there is an indication that the long-term trend in bottom pressure could be overestimated by the ECCO model used in the simulations due to a mass leakage (Condi and Wunsch, 2004). Future studies based on observations of full water column dynamic height at sites M3 and M1 together with satellite altimetry hold some promise to determine long-term trends in bottom pressure. Combined with overlapping data segments, this is expected to allow recovery of long period bottom pressure characteristics.

This study focused on demonstrating a capability to determine accurate geostrophic transport time series, while providing information on errors, instrument handling and data processing procedures. The mean velocity structure with depth and its origin have not been discussed. This, together with a thorough statistical analysis and a physical interpretation of the mechanisms of the observed fluctuations, is the subject of ongoing work. The present study is intended to establish a basis for future investigations and interpretations. This is especially relevant since long-term monitoring of large-scale geostrophic flow is becoming increasingly important, but has not been carried out to this extent and accuracy in the past. Small and easy to apply improvements will turn such systems into reliable tools for climate monitoring applications. The large scale integrated flows obtained by this technique could serve as useful constraints for ocean models, especially in the deep ocean where observations with high temporal resolution are rare.

When designing a MOC monitoring system, its life cycle cost (the sum of instrument acquisition, and aggregate maintenance costs) is an important factor. In an application at mid-latitudes with a baroclinic Rossby radius of less than 30 km, a current meter array spanning the whole transatlantic section would require 150 moorings to resolve the lateral scales of the flow. An end-point arrangement, even taking into account the topography of the Mid-Atlantic Ridge and the continental slopes, could be operated with about 10 moorings. The geostrophic end point technique is clearly advantageous over current meters in life cycle cost. The use of IESs rather than in situ T–S measurements in an end point array to infer dynamic height and thus internal transports would further reduce instrument costs, although the accuracy of this approach would have to be established. This method is particularly sensitive to the gravest vertical mode, i.e. usually a surface intensified baroclinic current. Therefore, as also suggested by results from Meinen and Watts (2000), it may not be particularly sensitive to deep internal transport in the ocean, which is essential when monitoring the MOC. At the MOVE mooring sites M1 and M3 the correlation between IES travel times and directly measured full water column averaged densities was typically less than 0.5. Using densities averaged between 1200 and 5000 dbar instead, the correlation with travel time dropped below 0.1.

Remote sensing is frequently referred to as a cost-effective alternative to in situ observations. Results from Latif et al. (2004) using a coupled general circulation model suggest that multidecadal fluctuations of the MOC could be inferred from the temporal evolution of subtropical North Atlantic sea surface temperatures (SST). However, findings from Collins et al. (2003) show that the correlation between MOC strength and North Atlantic SST varies significantly from model to model. Thus,

before large scale SST patterns from satellite observations can be used as a reliable proxy for the MOC, a statistically significant correlation between the two variables has to be demonstrated by in situ observations, which is one of the goals of MOVE. At the same time, MOVE serves as a ground-truth site for the validation of the space borne Gravity Recovery and Climate Experiment (GRACE), which is designed to observe temporal fluctuations of the Earth's gravity field. Over the oceans these can be converted into ocean bottom pressure fluctuations (e.g. Wahr et al., 2002). However, a comparison with MOVE in situ data suggests that the preliminary GRACE solutions overestimate the variability significantly (Kanzow et al., 2005) and thus may not be regarded as a reliable alternative to in situ measurements of bottom pressure for the study of the temporal evolution of the deep ocean flow field.

Acknowledgements

The authors would like to thank the captains and crews of the research vessels Knorr, Sonne, L'Atalante and Meteor for their assistance. The successful accomplishment of the mooring work would not have been possible without the competent and persistent commitment of C. Begler, U. Koy, R. Link, H. Moeller, G. Niehus, A. Pinck and many other colleagues. Support for the MOVE experiment and analysis were provided by the *Bundesministerium für Bildung und Forschung* within the German CLIVAR programme (Grant 03F0246A and 03F0377B) as well as by the *Deutsche Forschungsgemeinschaft* (Grant SE815/21). The critical comments of three anonymous reviewers helped to improve the manuscript substantially.

Appendix

How much of the long-term true ocean bottom pressure signal can be recovered from detrended and concatenated bottom pressure data segments? This is examined using two 8-year-long time series of bottom pressure (1995–2002) extracted from the $1^\circ \times 1^\circ$ ECCO (Estimating the Circulation and Climate of the Ocean) model (Stammer et al., 2003). This model version is constrained by observations such as satellite altimetry using the iterative adjoint technique. The two time series are displayed in Fig. A.1. They have been selected such that one location is close to mooring site M1 and the other is close to M3. Both time series show a long-term trend toward lower values and an annual cycle with an amplitude of 0.01 dbar.

The existence of seasonal and interannual signals in the time series offers a good opportunity to simulate the effect of detrending on the low-frequency fluctuations by cutting the 8-year model time series into segments of 1 or 2 year duration. An

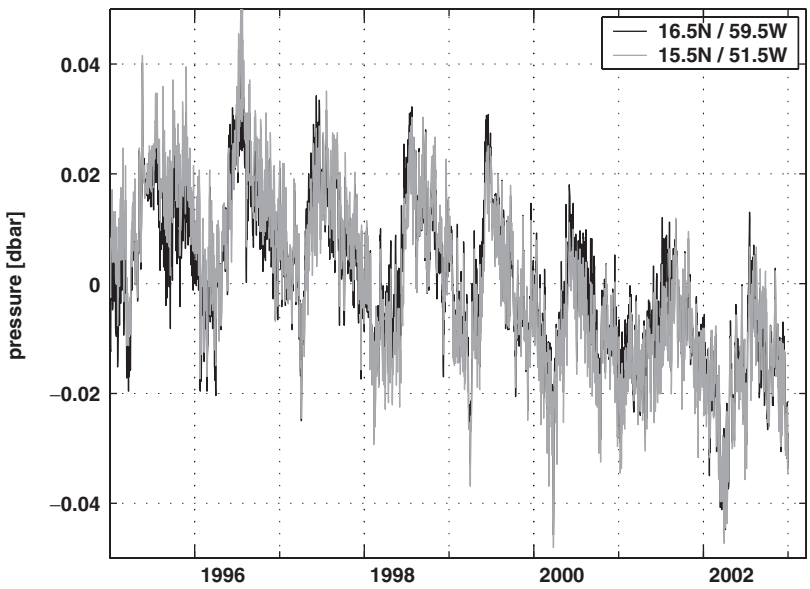

Fig. A.1. Bottom pressure time series from constrained ECCO model (time mean subtracted) from two locations in the tropical North Atlantic near MOVE sites M1 and M3.

artificial exponential-linear drift like the observed one (see Section 5) was added to each segment to simulate instrument drift during each deployment period. The drift coefficients A, B, C were defined by a random number generator within the observed limits, and are different for each data segment. Subsequently, for each segment the coefficients were estimated by applying a least squares procedure to the data. These will differ from the true A, B, C since oceanic signals affect the regression. The estimated drift is then subtracted from the raw data, which is exactly the procedure one would apply to actual observations. The data segment length and concatenation method for the segments has been varied as given in Table A.1. The bottom pressure difference (between M1 and M3) for the different cases is displayed in Fig. A.2. All of the time series are 60 day low-pass filtered in order to focus on the long-term variability. As expected, the short-term variability is not affected by detrending.

In the first case, which comes closest to the MOVE data analysis, a segment length of one year was chosen and the detrended segments were concatenated after simply subtracting the mean from each segment. Compared to the original time series (black line), variability at periods shorter than one year can be recovered. However, the amplitude of the annual cycle is weakened and the long-term trend cannot be recovered at all. The representation of the annual cycle improves drastically when choosing a 2-year segment length (red line). Of course, by subtracting the mean from each segment, the longer period signals are suppressed.

In the next test case, the segment length was kept at two years with segments overlapping each other for one year. This simulates a measurement strategy where one keeps two bottom pressure sensors at each site and alternately recovers and redeploys one of the instruments. By adjusting the overlapping time series, there is no need to subtract the mean

Table A.1
Effect of detrending and subsequent concatenation of data segments: the simulated cases differ in segment length and concatenation technique

Segment length	Segment concatenation technique	Color
1 year	Segment mean subtracted	Blue
2 year	Segment mean subtracted	Red
2 year	1 year overlap	Green
1 year	End-point matching	Magenta
2 year	End-point matching	Cyan

The color with which they are represented in Fig. A.2 is also given.

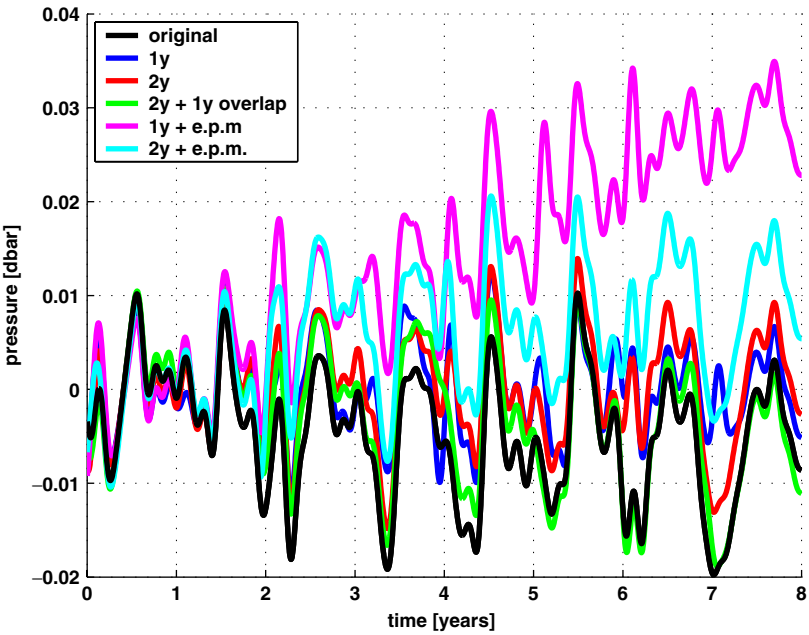

Fig. A.2. The black line represents the difference between the two month low pass filtered bottom pressure time series from the ECCO $1^\circ \times 1^\circ$ model displayed in Fig. A.1. The colored lines are the bottom pressure differences resulting from various detrending simulations defined in Table A.1. Each time series has been leveled such that the first year mean is set to zero.

from each time series. If the empirical drift removal worked perfectly in the sense that only the instrumental drift and no ocean signal would be affected, one would be able to recover the true long-term signals with this technique. The simulations (green line) show that the original long-term characteristics are by far best represented using this approach.

Finally, a simplified version of the end-point matching technique in which the data segments do not overlap was tested. The leveling of two segments is carried out such that the average of the first two months of the second segment corresponds to the mean of the last two months of the first segment. Theoretically, one should recover at least part of the true ocean long-term trend if the instrumental drift removal worked perfectly. In the simulation, this technique turns out to be very unreliable with either 1 or 2-year segments (magenta and cyan in Fig. A.2). The poor ability of the end-point matching technique to recover long-term variability is explained by the fact that errors in drift removal are generally largest at the segment end-points. The concatenation then results in a temporal integration of those errors, introducing arbitrary long-term trends. It should be noted that the end-point matching described by Whitworth and Peterson (1985) is not done using this objective criterion, but is carried out subjectively by eye. That might yield somewhat better results in some instances, but still is far from being a reliable tool for long-term trend assessment.

In conclusion, the simulations have shown that case 1 (annual segments with mean subtracted) yields good results at periods shorter than one year. The annual cycle is partly suppressed, and there is a complete lack of interannual variability. Doubling the segment length leads to an almost perfect recovery of the annual cycle, but only when allowing for a 1 year overlap of the segments is the long-term trend well represented. Endpoint matching cannot be recommended.

References

Berteaux, H., 1976. Buoy Engineering. Wiley, New York.

Book, J.W., Wimbush, M., Imawaki, S., Ichikawa, H., Uchida, H., Kinoshita, H., 2002. Kuroshio temporal and spatial variations South of Japan determined from inverted echo sounder measurements. Journal of Geophysical Research 107, doi:10.1029/2001JC000795.

Brown, W., Munk, W., Snodgrass, F., Mofjeld, H., Zetler, B., 1975. Mode bottom experiment. Journal of Physical Oceanography 5, 75–85.

Chave, A.D., Luther, D.S., Filloux, J.H., 1997. Observations of the boundary current system at 26.5 N in the subtropical North Atlantic Ocean. Journal of Physical Oceanography 27, 1827–1848.

Collins, M., Carril, A., Drange, H., Pohlmann, H., Sutton, R., Terray, L., 2003. North Atlantic Decadal predictability. Clivar Exchanges 28, 6–7.

Condi, F., Wunsch, C., 2004. Measuring gravity field variability, the geoid, ocean bottom pressure fluctuations, and their dynamical implications. Journal of Geophysical Research 109, doi:10.1029/2002JC001727.

Eden, C., Willebrand, J., 2001. Mechanism of interannual to decadal variability of the North Atlantic circulation. Journal of Climate 14, 2266–2280.

Filloux, J.H., 1980. Pressure fluctuations on the open ocean floor over a broad frequency range: new program and early results. Journal of Physical Oceanography 12, 1959–1971.

Helmbrecht, L., 2001. Entwicklung einer Verankerungssimulation als Designhilfe und zur Verbesserung der Datenanalyse—Diplomarbeit. Institut für Meereskunde, Kiel.

Hirschi, J., Baehr, J., Marotzke, J., Stark, J., Cunningham, S., Beismann, J.-O., 2003. A monitoring design for the Atlantic meridional overturning circulation. Geophysical Research Letters 30, 1413.

Hogg, N., 2001. Quantification of the deep circulation. In: Siedler, G., Church, J., Gould, J. (Eds.), Ocean Circulation and Climate. Academic Press, New York, pp. 259–270.

Hughes, C.W., Smithson, M.J., 1996. Bottom pressure correlations in the South Atlantic. Geophysical Research Letters 23 (17), 2243–2246.

Johns, W.E., Kanzow, T., Zantopp, R., 2005. Estimating ocean transports with dynamic height moorings: an application in the Atlantic deep western boundary current at 26.5°N. Deep Sea Research I 52 (8), 1542–1567.

Kanzow, T., 2000. Integrale Erfassung langperiodischer Transporte: Simulation und Optimierung eines verankerten Systems—Diplomarbeit. Institut für Meereskunde, Kiel.

Kanzow, T., 2004. Monitoring the integrated deep meridional flow in the tropical North Atlantic, Dissertation. Christian-Albrechts-Universität Kiel.

Kanzow, T., Flechtner, F., Chave, A., Schmidt, R., Schwintzer, P., Send, U., 2005. Seasonal variation of ocean bottom pressure derived from GRACE: local validation and global patterns, Journal of Geophysical Research 110, doi:10.1029/2004JC002510.

Latif, M., Roeckner, E., Botzet, M., Esch, M., Haak, H., Hagemann, S., Jungclaus, J., Legutke, S., Marsland, S., Mikolajewicz, U., Mitchell, J., 2004. Reconstructing, monitoring, and predicting decadal-scale changes in the North Atlantic thermohaline circulation with sea surface temperature. Journal of Climate 17, 1605–1614.

Lee, T.N., Johns, W.E., Zantopp, R., Fillenbaum, E.R., 1996. Moored observations of western boundary current variability and thermohaline circulation at 265°N in the subtropical North Atlantic. Journal of Physical Oceanography 26, 962–983.

Luther, D.S., Chave, A.D., 1993. Observing "integrating" variables in the ocean. In: Müller, P., Henderson, D. (Eds.), Proceedings of Seventh 'Aha Huliko'a Hawaiian Winter Workshop on Statistical Methods in Physical Oceanography, University of Hawaii, pp. 103–130

Lux, M., Mercier, H., Arhan, M., 2001. Interhemispheric exchange of mass and heat in the Atlantic ocean in January–March 1993. Deep Sea Research 48, 605–638.

Meinen, C.S., 2001. Structure of the North Atlantic current in stream-coordinates and the circulation in the Newfoundland Basin. Deep Sea Research 48, 1553–1580.

Meinen, C.S., Watts, D.R., 1998. Calibrating inverted echosounders equipped with pressure sensors. Journal of Atmospheric Oceanic Technology 15, 1339–1345.

Meinen, C.S., Watts, D.R., 2000. Vertical structure and transport on a transect across the North Atlantic Current near 42°N: time series and mean. Journal of Geophysical Research 105, 21869–21891.

Meredith, M.P., Vassie, J.M., Heywood, K.J., Spencer, R., 1996. On the temporal variability of the transport through Drake Passage. Journal of Geophysical Research 110, 22485–22494.

Pawlowicz, R., Beardsley, B., Lentz, S., 2002. Harmonic analysis including error estimates in MATLAB using T TIDE. Computational Geosciences 28, 929–937.

Pedlosky, J., 1987. Geophysical fluid dynamics. Springer, New York 624 pp.

Saunders, P.M., Mahrt, K.-H., Williams, R.T., 1991. Standards and laboratory calibration. WHP Operations and Methods, pp. 1–11.

Schmidt, H., 2004. Anwendung von Satellitenaltimetrie zur Verbessung von integralen in situ Transportmessungen—Diplomarbeit. Institut für Meereskunde.

SeaBird-Electronics, 2002. Compressibility compensation of seabird conductivity sensors. Application note, 10, 1–2.

Send, U., Kanzow, T., Zenk, W., Rhein, M., 2002. Monitoring the Atlantic meridional overturning circulation at 16°N. CLIVAR Exchanges 7, 1–4.

Stammer, D., Wunsch, C., Giering, R., Eckert, C., Heimbach, P., Marotzke, J., Adcroft, A., Hill, C.N., Marshall, J., 2000. The global ocean state during 1992–1997, estimated from ocean observations and a general circulation model. Part I: Methodology and state estimate. ECCO Report Series, (4), 53pp.

Stammer, D., Wunsch, C., Giering, R., Eckert, C., Heimbach, P., Marotzke, J., Adcroft, A., Hill, C.N., Marshall, J., 2003. Volume, heat and freshwater transports of the global ocean circulation 1993–2000, estimated from a general circulation model constrained by World Ocean Circulation Experiment (WOCE) data. Journal of Geophysical Research 108, doi:10.1029/2001JC001115.

Wahr, J., Jayne, S., Bryan, S., 2002. A method of inferring changes in deep ocean currents from satellite measurements of time-variable gravity. Journal of Geophysical Research 107, 3218.

Watts, D., Sun, C., Rintoul, S., 2001. A two-dimensional gravest empirical mode determined from hydrographic observations in the Subantarctic Front. Journal of Physical Oceanography 31, 2186–2209.

Watts, D.R., Kontoyiannis, H., 1990. Deep-ocean bottom pressure measurement: drift removal and performance. Journal of Atmospheric Oceanic Technology 7, 296–306.

Whitworth, T., 1983. Monitoring the transport of the Antarctic circumpolar current at Drake Passage. Journal of Physical Oceanography 13, 2045–2057.

Whitworth, T., Peterson, R.G., 1985. The volume transport of the Antarctic circumpolar current from bottom pressure measurements. Journal of Physical Oceanography 15, 810–816.